Journal Article

Hydrophobic derivatization of sodium alginate for use in fucoxanthin delivery

Han L, Zhai R, Williams PA, Hu B, Yang J, Dong N, Ban Y and Li T

Journal Pre-proof

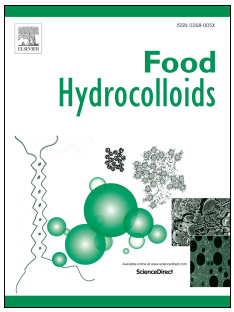

Hydrophobic Derivatization of Sodium Alginate for Use in Fucoxanthin Delivery

Lingyu Han, Ruiyi Zhai, Peter A. Williams, Bing Hu, Jixin Yang, Nuo Dong, Yujie Ban, Tingting Li

PII: S0268-005X(25)00624-1

DOI: https://doi.org/10.1016/j.foodhyd.2025.111664

Reference: FOOHYD 111664

To appear in: *Food Hydrocolloids*

Received Date: 20 December 2024

Revised Date: 11 June 2025

Accepted Date: 16 June 2025

Please cite this article as: Han, L., Zhai, R., Williams, P.A., Hu, B., Yang, J., Dong, N., Ban, Y., Li, T., Hydrophobic Derivatization of Sodium Alginate for Use in Fucoxanthin Delivery, *Food Hydrocolloids*, https://doi.org/10.1016/j.foodhyd.2025.111664.

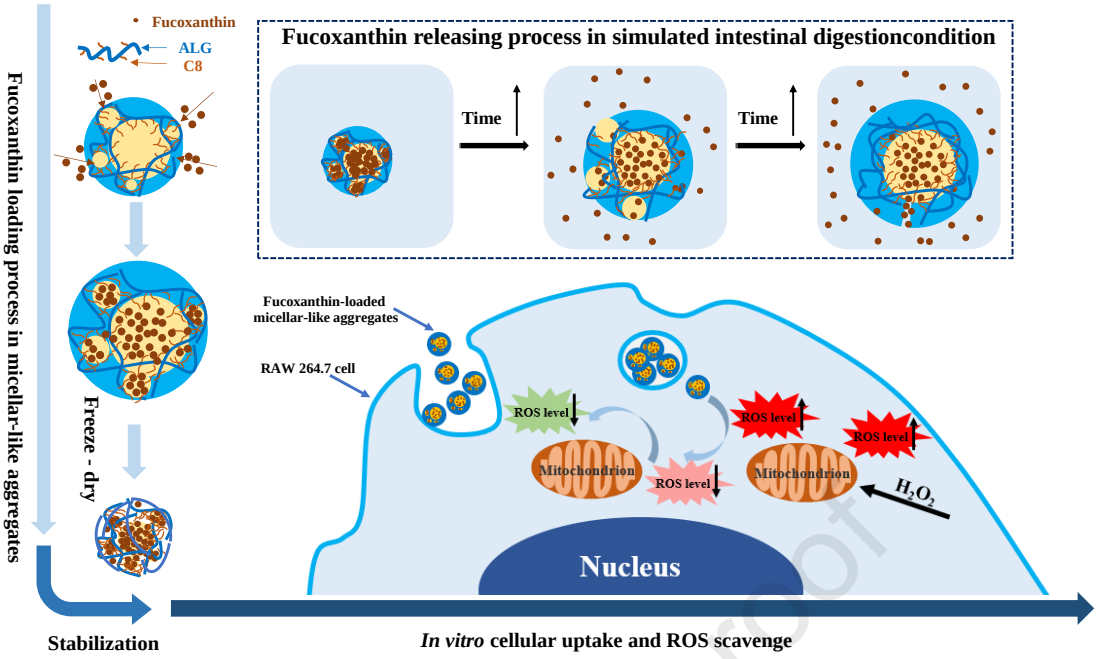

Hydrophobic Derivatization of Sodium Alginate for Use in Fucoxanthin Delivery

Lingyu Han[a, †], Ruiyi Zhai[a, †], Peter A. Williams[b,*], Bing Hu [a], Jixin Yang[b], Nuo Dong[a], Yujie Ban[a] and Tingting Li[a,*]

[a] *Key Lab of Biotechnology and Bioresources Utilization of Ministry of Education, College of Life Science, Dalian Minzu University, Dalian, Liaoning, 116600, China;*

[b] *Faculty of Life and Social Sciences, Wrexham University, Plas Coch, Mold Road, Wrexham, LL11 2AW United Kingdom;*

*Corresponding author:

Professor Peter A. Williams, Faculty of Life and Social Sciences, Wrexham University, Plas Coch, Mold Road, Wrexham, LL11 2AW United Kingdom.

Email: Pete.Williams@wrexham.ac.uk

Professor Tingting Li, Key Lab of Biotechnology and Bioresources Utilization of Ministry of Education, College of Life Science, Dalian Minzu University, Dalian, Liaoning, 116600, China.

Tel: +86-411-87656205, Email: jwltt@dlnu.edu.cn;

† These authors contributed equally to this work.

KEYWORDS: Sodium alginate; Hydrophobic modification; Fucoxanthin;

Encapsulation

ABSTRACT:

The present study successfully devised an innovative pH-sensitive system for encapsulating fucoxanthin, which effectively shielded RAW 264.7 cells from H_2O_2-induced damage. The formulation requires modification of sodium alginate with octanoyl chloride (C8) *via* esterification to provide amphiphilic self-assembly capacity of the system and loading of fucoxanthin *via* sonication. The hydration diameter (193.9 - 167.9 nm) and critical aggregation concentration of the micellar-like aggregates (1.4 - 0.5 mg/mL) gradually decreased with the increasing degree of substitution (1.54% - 60.20%). The encapsulation efficiency (46.11% - 88.54%) and loading capacity (4.61% - 8.85%) showed a positive correlation with the increasing degree of substitution. The TEM confirmed complete fucoxanthin encapsulation in micellar-like aggregates, forming smooth-surfaced spherical particles. *In vitro* simulated digestion assays demonstrated that micellar-like aggregates effectively shielded fucoxanthin from premature gastric release, while significantly improving its release efficiency during the intestinal phase. Fucoxanthin-loaded micellar-like aggregates endocytosed by RAW 264.7 cells alleviated cellular oxidative stress damage by reducing ROS levels. The study demonstrates the potential of self-assembled sodium alginate nanoparticles as a novel carrier for efficient delivery of hydrophobic substances, thereby establishing an innovative formulation for alleviating oxidative stress.

1. Introduction

Reactive oxygen species (ROS) are involved in both intracellular signaling and homeostasis (Hua, et al., 2023; Mensah, Kanwugu, Panda, & Adadi, 2023). Excess ROS production resulting from environmental factors, however, can induce oxidative stress with its associated damage (Roy, et al., 2024). This has led to a focus of attention on the use of natural orally administered antioxidants that could reduce oxidative damage by stimulating cellular defenses through ROS enzymatic conversions or scavenging of free radicals to alleviate oxidative stress (Jian, et al., 2017; Liu, Zhang, Fei, & Tan, 2024). Fucoxanthin, a carotenoid pigment isolated from marine algae, accounts for over 10.0% of natural carotenoids (Kuang, Ma, Guo, & Liu, 2024). It has a unique structure that includes an epoxide group, an allenic bond, and 9 double bonds, with conjugation of the latter contributing to the significant antioxidant properties of fucoxanthin (Han, et al., 2024). The allenic bond and 5,6-mono epoxide group allow the compound to function either directly or indirectly as a ROS scavenger to prevent oxidative damage to proteins, lipids, and deoxyribonucleic acid (DNA) by modulation of intracellular glutathione levels (Roy, et al., 2024). However, the highly unsaturated and hydrophobic structure of fucoxanthin contributes to its susceptibility to degradation due to increased light sensitivity, thermal instability, and vulnerability to oxidation (Adadi, et al., 2018). This results in the discoloration and loss of biological activity of fucoxanthin after extraction, thereby limiting its applications in the food industry (Tian, et al., 2024). Furthermore, during gastrointestinal digestion and absorption, fucoxanthin is unable to tolerate the acidic environment of the stomach, and its lipophilicity prevents its migration from the intestinal lumen to intestinal epithelial cells (Kuang, et al., 2024). These shortcomings present a challenge to absorption of fucoxanthin by the body, resulting in poor bioavailability. Advances in encapsulation technology have led to

improvements in the bioavailability of carotenoids, maximizing their biological functions by enhancing their solubility and stability (Yuan, Ma, & Zhang, 2023; Shavronskaya, et al. 2023).

Sodium alginate is an anionic polysaccharide with good biocompatibility, biodegradability, and lack of toxicity (Han, et al., 2024). Hydrophobic modifications of sodium alginate allow its use in the delivery of hydrophobic substances as the affinity is enhanced to enable their controlled release (Akshaya & Nathanael, 2024). In a previous study, we found that hydrophobic derivatization of sodium alginate influenced both encapsulation and release of fucoxanthin, with a negative association of the polysaccharide molar mass with both encapsulation efficiency (EE) and loading capacity (LC) of the aggregates (Han, et al., 2024).

In this study, sodium alginate and octanoyl chloride were utilized as raw materials for the synthesis of amphiphilic fatty acyl chloride-sodium alginate derivatives with different degrees of substitution through esterification reactions. Compositions and self-assemblies of the derivatives, together with the formation of micellar-like aggregates, were investigated using different techniques. Ultrasonic dialysis was used to encapsulate fucoxanthin in the aggregates, measuring both encapsulation efficiency (EE) and loading capacity (LC), together with an analysis of fucoxanthin release *in vitro*. The effects of these aggregates loaded with fucoxanthin in counteracting hydrogen peroxide were assessed in mouse RAW 264.7 macrophages, using fluorescence imaging to evaluate cell viabilities and ROS levels. The reason for choosing RAW 264.7 cells here was that H_2O_2-induced oxidative damage is often associated with immune system damage (Xie, et al., 2022). The objectives of this study focus on the construction of a nanomicellar sodium alginate-derivative carrier to encapsulate fucoxanthin, to enhance its stability, solubility, and rate of oral absorption,

providing a useful method for its use in functional foods. The strategy can also be applied to other hydrophobic materials in the food sector.

2. Materials and methods

2.1. Materials

Sodium alginate (9 kDa) was extracted as described in our previous study (Han, et al., 2024). Octanoyl chloride, formic acid, MTT, DCFH-DA, and fucoxanthin were purchased from Macklin Biochemical, with pyrene from Shanghai Aladdin Biochemical Technology, and D_2O from Alfa Aesar (Shanghai, China). PBS (pH 7.4) was from Sangon Biotech (Shanghai, China), and HCl, NaOH, absolute EtOH, DMSO, and KBr from Tianjin Kemiou Chemical Reagent Co. (Tianjin, China). RAW 264.7 cells were obtained from the Cell Bank of the Chinese Academy of Sciences (Shanghai, China). DMEM, penicillin-streptomycin, and fetal bovine serum (FBS) were from Gibco (Thermo Fisher, USA).

2.2. Preparation of sodium alginate derivative with different degrees of substitution

Formylation was conducted by mixing 100 mL of 1% (w/w, g/g) sodium alginate with formic acid (10 mL) for 30 min at 25℃. Octanoyl chloride (15, 18, 21, 25 mL, respectively) was then introduced drop by drop, after which the solution was heated to 50℃ for 30 min with constant stirring (100 rpm). The reaction was halted with 95% (v/v) ethanol. The mixture was then filtered to yield the derivatives, followed by washing in 95% ethanol and dialysis (cutoff 3500 Da) against distilled water for three days. The derivatives, namely, ALG-C8-1, ALG-C8-2, ALG-C8-3, and ALG-C8-4 according to the degree of substitution (DS) were obtained after freeze-drying.

2.3. Characterization of derivatives

Changes in the sodium alginate structure and its associated mechanisms induced by hydrophobic modifications were assessed following our previously applied methods

(Han, et al., 2024). After dissolution in D_2O, ^1H NMR spectra were acquired with an ULTRASHIELD 400 PLUS spectrometer (Bruker, USA) and MestreNova software for subsequent analysis. FTIR spectroscopic measurement was performed on an FTIR spectrometer (Shimadzu, Japan). Specifically, samples with KBr powder were ground and pressed into tablet form, after which 64 FTIR spectra were acquired over 500-4000 cm^{-1} at 4 cm^{-1} resolution. X-ray diffraction (XRD-6000 system, Shimadzu, Japan) was used to assess the structures of sodium alginate and its derivatives with Cu Kα radiation at 40 kV and 40 mA. The rate of scanning was 2°/min in 5-60° range. Thermal gravimetric analysis (TGA) was conducted using an SDT 650 (TA, USA) thermogravimetric analyzer by heating the samples to 30-600℃ at a rate of 20℃/min. Derivative thermogravimetric (DTG) is the first-order derivatives of weight loss.

2.4. Critical aggregation concentration (CAC)

2.4.1. Fluorescence measurements

Self-assembly of the amphiphilic derivatives was examined with pyrene fluorescence probes as previously described to determine the critical aggregation concentration (CAC) (Han, et al., 2024). Fluorescence spectra of the mixtures of samples and pyrene were acquired with an FS5 fluorescence spectrophotometer (Edinburgh Instruments, UK) after overnight storage at 25℃. Emission spectra (350-450 nm) were obtained following pyrene excitation at 334 nm, with respective excitation and emission slit openings of 5 and 2.5 nm.

2.4.2. Dynamic light scattering (DLS)

CAC was determined from the slope of the graph of aggregate size versus concentration as described in a previous report (Han, Ratcliffe, & Williams, 2015). DLS was performed using a Zetasizer Nano ZS (Malvern Instruments, UK) using serial dilutions of 2 mg/mL stock solutions for sample preparation, followed by filtration

(0.45 μm).

2.4.3. Surface tension (ST)

Static ST values of ALG-C8 solutions were measured using a surface tension meter (HengPing BZY-1, Shanghai, China) (Han, et al., 2023). Three measurements were collected at 25 ± 1°C. CAC values were measured from the slope of the graph of equilibrium ST versus concentration. Micellization of the derivatives was examined by Gibbs adsorption. From the graph of ST versus the natural logarithm of the solution concentration, the surface excess (Γ) and molecular area (A) were determined with Equations (1) and (2):

$$\Gamma = -\frac{1}{RT}\frac{d\gamma}{d\ln c} \quad (1)$$

$$A = \frac{1}{\Gamma N} \quad (2)$$

where R is the gas constant, N is Avogadro's number, γ is the ST, T is the temperature, and C is the concentration.

2.5. Aggregate sizes and zeta potentials

These were determined at 25°C using the Zetasizer Nano ZS as mentioned above. Samples (2 mg/mL) were filtered (0.45 μm) before measurement in triplicate.

2.6. Synthesis and characterization of fucoxanthin-loaded micellar-like aggregates

Derivatives (100 mg) were dissolved in 50 mL of DI water. 5 mL solution of fucoxanthin in ethanol (2 mg/mL) was introduced to the derivative solutions and ultrasonicated for 30 min followed by dialysis (cutoff 3500 Da) against DI water for 48 h, and subsequent freeze-drying.

The freeze-dried fucoxanthin-loaded aggregates (1 mg) were dissolved in 10 mL of ethanol, sonicated for 30 min, and filtered (0.45 μm). Fucoxanthin concentrations were measured at 450 nm in a UV-vis spectrophotometer (UV-6100, MAPADA, China) using standard curves as described previously (Han, et al., 2024). The EE and LC were

172 determined by equations (3) and (4), respectively:

173 $$\mathrm{EE}\ (\%) = \frac{\text{weight of fucoxanthin in micellar-like aggregates}}{\text{weight of fucoxanthin fed initially}} \times 100\% \quad (3)$$

174 $$\mathrm{LC}\ (\%) = \frac{\text{weight of fucoxanthin in micellar-like aggregates}}{\text{weight of micellar-like aggregates containing fucoxanthin}} \times 100\% \quad (4)$$

175 ***2.7. Transmission electron microscopy (TEM)***

176 Following evaporation of the sample solutions (2 mg/mL) on a copper grid with
177 carbon coating, the aggregates were stained with phosphotungstic acid and examined
178 by TEM (JOEL JEM-2100, Japan). The size of the aggregates was analyzed by Image
179 J software.

180 ***2.8. Fucoxanthin release in simulated gastric and intestinal conditions***

181 The fluids were prepared as described in Han, et al. (2024). Solutions of fucoxanthin-
182 loaded aggregates (2 mg/mL) were added to equal volumes of simulated gastric fluids,
183 with adjustment of the pH to 2.0, followed by stirring (100 rpm) for 2 h at 37℃.
184 Aliquots (2 mL) were collected at various times and filtered (0.45 μm) into UV-grade
185 cuvettes. 30 mL solution was incubated in a 37℃ water bath with the introduction of
186 1.5 mL of the intestinal fluid (containing 10 mM $CaCl_2$ and 150 mM NaCl), 4 mL of
187 bile salts (46.9 mg/mL) and 4 mL of lipase (187.5 mg/4 mL, freshly prepared), and the
188 pH was adjusted to 7.0. After stirring (100 rpm) for 2 h in the water bath, the UV-vis
189 absorbance was measured as described above.

190 ***2.9. In vitro cytotoxicity of the sodium alginate derivatives with different degrees of***
191 ***substitution***

192 Cytotoxicity of the derivatives was determined using MTT assays as described in
193 Tian, et al. (2024) with minor changes. RAW 264.7 cells (1×10^4/well) were inoculated
194 in 96-well plates and grown at 37℃ with 5% CO_2 for 24 h after which the DMEM
195 complete medium (containing 1% penicillin-streptomycin and 10% FBS) were
196 substituted by the fresh ones with varying sample amounts (0, 200, 400, 600, 800, and

1000 μg/mL) for further incubation for 24 h. MTT reagent (5 mg/mL, 20 μL/well) was incubated for 4 h. After removal of the media, 150 μL of DMSO per well was added and absorbances at 490 nm were measured with a microplate reader (Synergy H1, Biotek, Paramus, NJ, USA) after 15 min of vigorous shaking. Viability (%) was assessed using Equation (5):

$$\text{Cell viability (\%)} = \frac{At-Ac}{Au-Ac} \times 100\% \quad (5)$$

where At and Au represent respective absorbances at 490 nm with and without samples, and Ac is the control without cells.

2.10. Protective effects of fucoxanthin-loaded aggregates on oxidative stress in RAW 264.7 cells

2.10.1 Establishment of RAW 264.7 cells H_2O_2 model

Damage to RAW 264.7 cells caused by exposure to H_2O_2 was evaluated by measuring cell viability using MTT assays (Lv, et al., 2022). RAW 264.7 cells (1×10^5/well, 200 μL) were grown in 96-well plates for 24 h. After discarding the media, cells were exposed to H_2O_2 of various concentrations of 0-800 μmol/L in complete DMEM for 24 h.

2.10.2 Protection against H_2O_2-induced oxidative damage

RAW 264.7 cells (1×10^5/well) were inoculated in 96-well plates and grown for 24 h. Media were then replaced with the ones containing 500 μM H_2O_2 and varying amounts (0, 50, 100, 150, 200, 250 μg/mL) of fucoxanthin-loaded aggregates and grown for another 24 h, after which cell viability was assessed using MTT assays.

2.10.3 ROS measurements

ROS contents of RAW 264.7 cells were examined with DCFH-DA (Wang, et al., 2018). RAW 264.7 cells (1×10^5/well) were inoculated in 96-well plates and grown for 24 h. The media were then substituted with fresh ones with 500 μM H_2O_2 and

fucoxanthin-loaded aggregates (250 μg/mL) and grown for a further 24 h. The media were aspirated and 200 μL of DCFH-DA (10 μM) was added for 1 h followed by measurement of the fluorescence intensity with a Synergy H1 microplate reader (Biotek, USA) using 485 nm (excitation) and 520 nm (emission) wavelengths.

2.11. Cellular uptake

Cellular uptake was assessed as described by the previous report (Han, Sun, Williams, Yang, & Zhang, 2022) with several modifications. RAW 264.7 cells (5×10^5/dish) were inoculated in glass-bottomed confocal dishes and grown for 24 h. Sample solutions were mixed with DMEM to final fucoxanthin concentrations of 2.3 μg/mL and added to the dishes after removal of the original media, with incubation for 30 min or 4 h. After removal of the media and three rinses with PBS (pH 7.4), the cells were fixed with paraformaldehyde (500 μL, 4%) for 30 min and subsequently washed with PBS. Nuclei were counterstained with DAPI (200 μL, 10 min) in the dark followed by washing with PBS. Fluorescence was assessed and imaged using an Olympus FV10-ASW confocal laser scanning microscope (CLSM) with quantification using Image J software. The excitation and emission light of fucoxanthin at 488 nm and 710 nm, respectively (Fan, et al., 2021).

2.13. Statistical Analysis

All samples were prepared in triplicate and all experiments were carried out in triplicate for each sample. All data are presented as mean ± standard deviation. One-way ANOVA tests were used in SPSS 26.0 software for comparisons with a significance level of $P < 0.05$.

3. Results and discussion

3.1. Synthesis and analysis of sodium alginate derivatives

The ^{1}H NMR spectra of sodium alginate and sodium alginate derivatives are

illustrated in Fig. 1a. The peaks within the range of 3.2 to 4.0 ppm correspond to hydrogen shifts in the backbone of sodium alginate which is the same as our previous research, as reported by Han et al. (2024). The spectra of the derivatives are similar, with specific peaks at 0.8, 1.2, 1.6, and 2.4 ppm ascribed to the presence of protons on octanoyl chloride methyl and methylene groups (Han, Ratcliffe, & Williams, 2017). The resonance peak at 4.79 ppm is due to the presence of the water solvent (D_2O). These results confirmed the successful grafting of octanoyl chloride onto sodium alginate through esterification reactions. DS values were determined using our previously established methodology (Han et al., 2024) (Table 1). These values, shown as the molar percentages of alkyl chains of sugar units, ranged from 1.54% to 60.20%.

Changes in structure induced by the derivatisation were assessed using FTIR spectroscopy (Fig. 1b). Sodium alginate contributed absorption peaks at 3400, 1645, and 1405 cm^{-1}, ascribed to stretching vibrations of hydroxyls and the asymmetric and symmetric stretching vibrations of carboxylates, respectively (Liu, et al., 2024). The spectra of the derivatives showed new peaks at 1739 and 1560 cm^{-1}, indicative of new ester linkages between octanoyl chloride and sodium alginate (Han, et al., 2024). These results confirmed the success of the alkyl chain incorporation.

Structural changes were also evaluated using XRD, as shown in Fig. 1c. The overall structure of the polymer has significant effects on the stability, encapsulation, and release of the incorporated substance, with amorphous structures having marked effects on substance delivery (Han, et al., 2024). The crystal structure of sodium alginate was characteristic, resulting from hydrogen bonding within the molecule, seen in the noticeable diffraction peaks at 14.0° and 22.0° (Liu, et al., 2022). The broad amorphous peak at 2θ = 15-25° suggested that the octanoyl chloride grafting disrupted uronic acid hydrogen bonding on sodium alginate and reduced the rigidity of the molecule (Liu, et

al., 2024). Additionally, the diffraction peak at 2θ = 15-25° in the non-crystalline area was strengthened as the DS increased, suggesting the successful attachment of more alkyl chains (Liu, et al., 2024).

Thermal stability was evaluated using TGA (solid line in Figure 1d.) and DTG (dashed line in Fig. 1d.). The thermal degradation of the derivatives resembled that of sodium alginate, seen in weight losses at 50-150℃ and 200-300℃ respectively. The first phase is due to the volatilization of water within the samples (Han, et al., 2024). The weight loss of the sodium alginate derivatives, resulting from temperature-induced degradation of the polymer molecule during the second phase, were all more than that of sodium alginate. The DTG results indicated that sodium alginate and its derivatives exhibited a high rate of weight change within the temperature range of 200-300℃. These results indicated the destruction of the sodium alginate crystal structure and hydrogen bonding by the addition of alkyl chains in the derivatives, thus lowering their thermal stability. This is indirect evidence of the successful grafting of octanoyl chloride onto the sodium alginate by esterification reactions.

3.2. Self-assembly of micellar-like aggregates

Esterification results in the introduction of long hydrophobic carbon chains onto the hydrophilic sodium alginate; the derivatives are thus amphiphilic and can undergo self-assembly into micellar-like aggregates in aqueous solutions. The CAC values of the aggregates were determined using three methods. First, self-assembly was evaluated by the quantification of CAC using a pyrene fluorescence probe. At low concentrations, I_1/I_3 was found to be approximately 1.8, indicative of the presence of a polar aqueous environment. As the concentration of the samples was raised, the I_1/I_3 value declined, resulting from the formation of micellar-like structures with hydrophobic cavities in which the pyrene was enclosed, consistent with previous findings on amphiphilic block

297 copolymers (Han, et al., 2024). The CACs for ALG-C8-1, ALG-C8-2, ALG-C8-3, and
298 ALG-C8-4 were 1.4, 1.1, 0.9, and 0.5 mg/mL, respectively (Fig. 2a). The lowest value
299 was thus seen in ALG-C8-4 which had the highest DS of the hydrophobic groups,
300 indicating that its micellar-like aggregates were more stable in diluted conditions (Liu,
301 et al., 2024).

302 Second, Fig. 2b shows a plot of the hydrodynamic diameters of the derivatives in
303 solution against concentration. The micellar-like aggregates are formed by self-
304 assembled amphiphilic polymers in aqueous solution. At low concentrations, these
305 polymers can be detected in unimer states (Bu, et al., 2021), while raising
306 concentrations to near the CAC results in aggregation and increased hydration
307 diameters. The CACs for ALG-C8-1, ALG-C8-2, ALG-C8-3, and ALG-C8-4
308 determined from changes in the slopes of the curves were 1.43 ± 0.06, 1.17 ± 0.06, 0.76
309 ± 0.05, and 0.64 ± 0.04 mg/mL, respectively.

310 Third, the ST values of the samples in relation to concentration are presented in Fig.
311 2c. The amphiphilic derivatives are able to counteract repulsive forces in the interfacial
312 area and thus lower the free energy. The CAC values were determined from the curve
313 inflection. As shown in Table 1, these values declined as the DS of the samples
314 increased, yielding 1.37 ± 0.03, 1.12 ± 0.07, 0.73 ± 0.06, and 0.6 ± 0.05 mg/mL,
315 respectively, essentially consistent with the values above. This is likely the result of the
316 higher polarity seen in derivatives with higher DS values resulting from reduced ST.
317 These findings demonstrated that increases in the DS of the derivatives led to
318 corresponding reductions in their CAC. Increases in DS reduce the hydration of
319 hydrophilic groups, promoting micellization. The surface excess value (Γ) is an
320 indicator of the difference in concentration between the surface and bulk solutions
321 resulting from adsorption, while the molecular area (A) represents the area taken up by

one molecule at the interface (Hua, et al., 2021). Higher Γ and A values indicate greater molecular compaction at the interface (Han, et al., 2024). The surface excess value is obtained from the slope of the γ-ln C curve immediately below the CAC, as illustrated in Fig. S1 (see supplementry data). The derivatives showed surface excess values between 0.08 and 0.12× 10^{-6} mol/m^2, with areas per molecule ranging from 0.14 to 0.20 nm^2 (Table 1). ALG-C8-4 had both the highest DS and Γ values, together with the lowest A values, indicative of dense packing of molecular aggregates at the surface (Barai, et al., 2019), resulting from greater stacking of the aggregates at the interface due to the formation of monolayers under the action of intermolecular forces. It is thus proposed that the DS influenced both the adsorption and the degree of compaction of the aggregates at the interface, thus determining the interfacial parameters, namely, ST, CAC, Γ, and A. Meanwhile, the Γ and A values for ALG-C8-1 were 0.08 mol/m² and 0.20 nm², respectively, which are consistent with the results of previous studies reporting 0.08 mol/m² and 0.21 nm² of ALG(9kDa)-C8 with the same DS and molar mass (Han et al., 2024).

3.3. Characterization of blank and fucoxanthin-loaded aggregates

The particle sizes and zeta potentials of the aggregates (2.0 mg/mL) were determined using DLS; the results are presented in Table 1. Increasing DS of the derivatives reduced the aggregate sizes from 193.9 ± 2.40 nm to 167.9 ± 2.21 nm. Thus, aggregate size was negatively associated with DS. At similar concentrations, the particle sizes of the aggregates decreased gradually as the DS increased, essentially due to the greater contents of octanoyl chloride that promoted intermolecular association through hydrophobic π-π interactions, thus enhancing the compaction of the inner hydrophobic core and reducing the overall size of the aggregate (Liu, et al., 2024). The aggregates size of ALG-C8-1 aligns with the findings (193.9 ± 0.80 nm) from prior studies (Han

et al. 2024). The zeta potential is important in the maintenance of the stability of the micellar structure; this was found to have an electronegativity above -30.0 mV which contributed to micellar stability due to the presence of higher electrostatic repulsive forces between the particles (Han, et al., 2024). The information shown in Table 1 indicates that the zeta potentials of all the samples were above -30.0 mV, indicative of the excellent stability of the aggregates formed from the sodium alginate derivatives. The zeta potential of ALG-C8-1 was -31.3 ± 0.04 mV is nearly the same as the value of our previous data which is -31.4 ± 0.10 mV (Han, et al., 2024).

Table 1 details the EEs and LCs of the samples. It is apparent that increases in the DS values of the derivatives are associated with increases in both values in the aggregates. The EE and LC of the ALG-C8-1 aggregates were 46.11 ± 2.22% and 4.61 ± 0.22%, respectively. In our previous study (Han et al., 2024), the EE and LC of ALG(9 kDa)-C8, which had a similar DS of 1.53% and a molar mass of 9 kDa, were 95.8 ± 0.75% and 4.6 ± 0.04%, respectively. When considering micellar-like aggregates at the same concentration (2 mg/mL), the drug loading in this experiment was doubled to 10 mg (5 mL solution of 2 mg/mL fucoxanthin in ethanol), compared to 5 mg in the previous work. Theoretically, the EE value of ALG-C8-1 in this experiment should be approximately half of the previous value, while the LC value should remain unchanged. Within the margin of error, the experimental results are consistent with the theoretical expectations. The highest EE and LC values were seen in the ALG-C8-4 aggregates, which were 88.54 ± 1.14% and 8.85 ± 0.11%, respectively. These findings indicated that increased DS is associated with a corresponding enhancement of the hydrophobic interactions, with the fucoxanthin molecules binding more tightly within the hydrophobic core region, thus increasing the EE and LC values (Liu, et al., 2024). The presence of greater numbers of hydrophobic side groups on the derivatives would lead

372 to the formation of increased numbers of hydrophobic microdomains with greater
373 density. The ALG-C8-4 derivatives were found to form the highest number of
374 aggregates with the smallest sizes in aqueous solutions, thus having the greatest surface
375 areas and highest embedding capacity (Han, et al., 2024). The higher EE and LC values
376 are associated with reduced loss of fucoxanthin, thus lowering the cost of preparation
377 of fucoxanthin-loaded aggregates.

378 The morphology of fucoxanthin-loaded (2.0 mg/mL) and blank aggregates was
379 compared using TEM. As illustrated in Fig. 3, the aggregates were observed to disperse
380 well. However, comparison of the particle sizes of the aggregates (2.0 mg/mL) between
381 the TEM and DLS results (Table 1.) showed that the particle sizes determined by TEM
382 with average respective sizes of 26.7, 23.1, 19.8, and 17.0 nm according to the different
383 DS values were smaller. It was attributed to the characteristics of the sample preparation,
384 with the samples examined by TEM being completely dry, resulting in shrinking of the
385 aggregates due to evaporation of water. The trend observed in the TEM results mirrors
386 that of the DLS results, indicating a decrease in aggregate size as the DS increases.

387 In contrast, the aggregates in solution were immersed in water and thus expanded in
388 the surrounding solution, resulting in larger particle sizes than those observed for dried
389 aggregates (Liu, et al., 2024). The average sizes of the fucoxanthin-loaded aggregates
390 were 40.0, 35.6, 28.6, and 24.2 nm, respectively, slightly greater than those of the blank
391 aggregates. This suggests the successful encapsulation of fucoxanthin within the
392 aggregate structures. The aggregate size and fucoxanthin-loaded aggregate size of
393 ALG-C8-1, as determined by TEM, are largely consistent with the previously reported
394 values of 22.1 nm and 39.6 nm, respectively (Han et al., 2024).

395 ***3.4. Fucoxanthin release from aggregates in vitro***

396 Based on our previous study (Han et al. 2024), the release of fucoxanthin from the

aggregates was evaluated under conditions simulating those of the gastrointestinal tract, with the results depicted in Fig. 4a. Fig. 4b shows fucoxanthin release in the simulated system at varying time points. There was no release of unencapsulated fucoxanthin due to the absence of free fatty acid formation, nor was there any increased release in the simulated gastric environment. The images revealed that the samples exhibited no release of fucoxanthin within the gastric environment for a duration of up to 120 min. This was most likely the result of protonation of the sodium alginate carboxyl group, enhancing the hydrophobicity of the polymer at pH 2.0. This led to self-assembly of the hydrophobic chains, forming dense structures in aqueous media resulting from more intense hydrophobic interactions both within and between the molecules, maintaining the compact and tight structure for extended periods (Han, et al., 2024). Thus, acidic conditions are associated with reduced rates of fucoxanthin release from the aggregates. This differed from the simulations of the small intestinal environment, where increases in absorbance, indicative of fucoxanthin release, were seen after incubation for 10 min. This is the result of electrostatic repulsion between ionized carboxylates within the aggregates, leading to swelling and overall relaxation of the structure and thus the release of fucoxanthin, consistent with previous findings (Han, et al., 2024). The amphiphilicity of derivatives with high DS values and shorter hydrophobic chains allows the formation of aggregates characterized by a mixture of hydrophilic and hydrophobic areas, in contrast to aggregates with low DS values, as described previously (Han, et al., 2024; Wu, Li, Zhao, Ye, & Zhao, 2022). The sharp increases in fucoxanthin release observed within the initial 40 min of simulated digestion under intestinal conditions are likely due to the presence of numerous microdomains within the fucoxanthin-loaded aggregates (Liu, et al., 2022). The rate of release subsequently plateaued, due to fucoxanthin release from the aggregate cores (Liu, et al., 2024). The

absorbances and images of the filtrate solutions confirmed that samples with the highest LC values released the largest amount of fucoxanthin in the intestinal simulations. These findings indicated that the fucoxanthin-loaded aggregates can pass through the stomach intact, releasing the encapsulated fucoxanthin in the intestine in a controlled manner. It is important that effective nano-delivery systems used in oral applications remain intact within the acidic gastric environment, releasing their contents when entering the more alkaline conditions of the small intestine (Kuang, et al., 2024).

3.5. Cytotoxicity of sodium alginate derivatives in vitro

The cytotoxicity of the sodium alginate and sodium alginate derivatives was assessed in RAW 264.7 cells using MTT assays. It is generally considered that cell viability >80% represents low cytotoxicity when used with MTT assays (Liu, et al., 2022). Fig. 5 demonstrates that as the concentration of the derivatives increases, the cell viability of RAW 264.7 cells remains above 90% without significant differences ($P > 0.05$). This indicated that the presence of the alkyl chains did not lead to cytotoxicity, even at derivative concentration of 1000 μg/mL. All samples fall within the biologically safe range at this concentration level. Notably, this biocompatibility was not dependent on either the amount or DS values of the derivatives. These results suggest that the derivatives would be suitable for other applications in the delivery of different hydrophobic compounds, largely the consequence of the specific attributes of sodium alginate, including their biocompatibility, biodegradability, and non-toxicity (Liu, et al., 2021). These findings echo with those of other studies on the synthesis and properties of amphiphilic sodium alginate derivatives (Liu, et al., 2021; Liu, et al., 2022).

3.6. Protection against H_2O_2-induced oxidative damage

Cultured cells are frequently used to examine and quantify the antioxidant properties of bioactive substances (He, Zhu, Yin, & Yang, 2022). The present study used H_2O_2 as

447 a generator of free radicals to promote oxidative stress in RAW 264.7 cells to investigate
448 the protective influence of the fucoxanthin-loaded aggregates against both oxidative
449 stress and inflammation (Fig. 6a). H_2O_2 may lead to cellular injury either through direct
450 oxidative effects on cellular lipid, protein, and DNA constituents, or indirectly by
451 functioning as a signaling molecule triggering cell death-associated pathways (Wang,
452 et al., 2018). As illustrated in Fig. 6b, treatment of RAW 264.7 cells with H_2O_2 resulted
453 in concentration-dependent reductions in cell viability. Incubation with 500 μM H_2O_2
454 for 24 h resulted in an overall viability of 53.4%, relative to the controls. In the
455 subsequent experiment, 500 μM H_2O_2 was introduced to the cells for 24 h to determine
456 whether the fucoxanthin-loaded aggregates could protect against oxidative injury in the
457 cells. As illustrated in Fig. 6c, fucoxanthin strongly reduced the levels of oxidative
458 injury from H_2O_2, with dose-dependent effects. At fucoxanthin concentration of 200
459 μg/mL within the aggregates, the level of oxidative damage was equal to that of the
460 control. In an analysis of the antioxidant effects of fucoxanthin, Liu, et al. (2024)
461 reported that its antioxidant properties were due to its specific electron-rich structure,
462 and that the compound was effective in protecting cells from injury resulting from H_2O_2
463 exposure by increasing the levels of glutathione and antioxidant enzymes in the cells.
464 Exposure to exogenous H_2O_2 leads to imbalances in the intracellular redox system,
465 overwhelming endogenous antioxidant defenses and resulting in excessive ROS
466 accumulation (Liang, et al., 2021). Thus, measurement of ROS levels can provide
467 information on the extent of oxidative damage. Here, ROS levels were examined using
468 the fluorescent probe DCFH-DA (Fig. 6d). Relative to the controls, it was found that
469 H_2O_2 exposure enhanced ROS production, shown by the intensity of fluorescence in
470 the cells. This fluorescence was reduced by incubation with fucoxanthin-loaded
471 aggregates, with fluorescence intensity showing negative correlation with the

fucoxanthin content of the samples. These findings demonstrate that fucoxanthin-loaded aggregates possess potent antioxidant properties capable of mitigating oxidative stress-induced damage.

3.7. Assessment of cell uptake in vitro

The uptake of fucoxanthin by RAW 264.7 cells was assessed by CLSM (Fig. 7a). The cells were treated with the fucoxanthin-loaded aggregates for 30 min and 4 h, respectively, and were then examined and imaged with CLSM (Fig. 7b). Red fluorescence associated with fucoxanthin was visible after 30 min in the different groups, indicating effective uptake of the fucoxanthin-loaded aggregates by the cells. This intracellular fluorescence was markedly induced after 4 h of incubation, indicative of constant uptake of the aggregates by the cells in a time-dependent manner. The most intense fucoxanthin fluorescence was seen with the ALG-C8-4 aggregates compared with the other samples, indicating that fucoxanthin delivery to the cytoplasm was more efficient with aggregates with smaller particle sizes. The CLSM images are in agreement with the quantification of fluorescence intensity (Fig. 7c). It is evident that the fluorescence absorption of ALG-C8-4 aggregates is strongest at 0.5 hours and 4 hours, with a significant difference observed between other ALG-C8 samples. With the increasing degree of DS, the delivery of fucoxanthin to the cytoplasm became more efficient. These findings demonstrated that the fucoxanthin-loaded aggregates were effectively taken up by cells and showed good biocompatibility. Small molecules interact with components of the cell membrane, entering the cells through various endocytic pathways. Depending on the specific mechanism involved, endocytosis can be classified as phagocytosis, pinocytosis, or receptor-mediated endocytosis (Zhang, et al., 2024). Uptake of carotenoids, for instance, occurs via the dectin-1 receptor or by passive diffusion (Liu, et al., 2024; Zhang, et al., 2024). Thus, the identification of the

specific mechanism underlying fucoxanthin uptake is complex, and the process could be mediated by different mechanisms within a single cell. The results of this investigation provide a basis for future elucidation of the method by which fucoxanthin-loaded sodium alginate-based aggregates are taken up by cells.

4. Conclusion

This study describes a novel strategy for the synthesis of uniformly sized fucoxanthin-loaded sodium alginate-based micellar-like aggregates capable of pH-sensitive. The sizes of the aggregates were in the range of 100-200 nm. *In vitro* studies using simulation digestive systems indicated that the fucoxanthin was protected by the aggregates in acidic conditions of the stomach followed by release on reaching the more alkaline environment of the small intestine. Cytotoxicity and uptake assays demonstrated a lack of cytotoxicity with effective cellular uptake of both blank and fucoxanthin-loaded aggregates. Furthermore, fucoxanthin-loaded aggregates protected cells against H_2O_2-induced oxidative damage and reduced the levels of intracellular ROS. These results suggest the potential of sodium alginate-based micellar-like aggregates as effective carriers for delivering hydrophobic fucoxanthin or other functional molecules.

Credit Author Statement

Lingyu Han: Methodology, Formal analysis, Investigation, Writing-original draft, Writing review and editing

Ruiyi Zhai: Methodology, Investigation, Writing-original draft, Writing review and editing

Peter A. Williams: Conceptualization, methodology, formal analysis, Writing review and editing

Bing Hu: Conceptualization, methodology, Writing review and editing

Jixin Yang: Conceptualization, methodology, Writing review and editing

Nuo Dong: Conceptualization, methodology, Software

Yujie Ban: Conceptualization, methodology, Software

Tingting Li: Conceptualization, methodology, Writing-original draft, Writing review and editing

Declaration of competing interest

The authors declare that they have no conflicts of interest regarding this work.

Acknowledgements

This work was supported by the 14th Five-Year national key research and development plan project (2024YFD2401605).

List of Figures

560 fucoxanthin in RAW 264.7 cells by Image J software. Data are presented as mean ± SD.

561 Different lowercase letters indicate significant differences ($P < 0.05$).

562

563

564

565

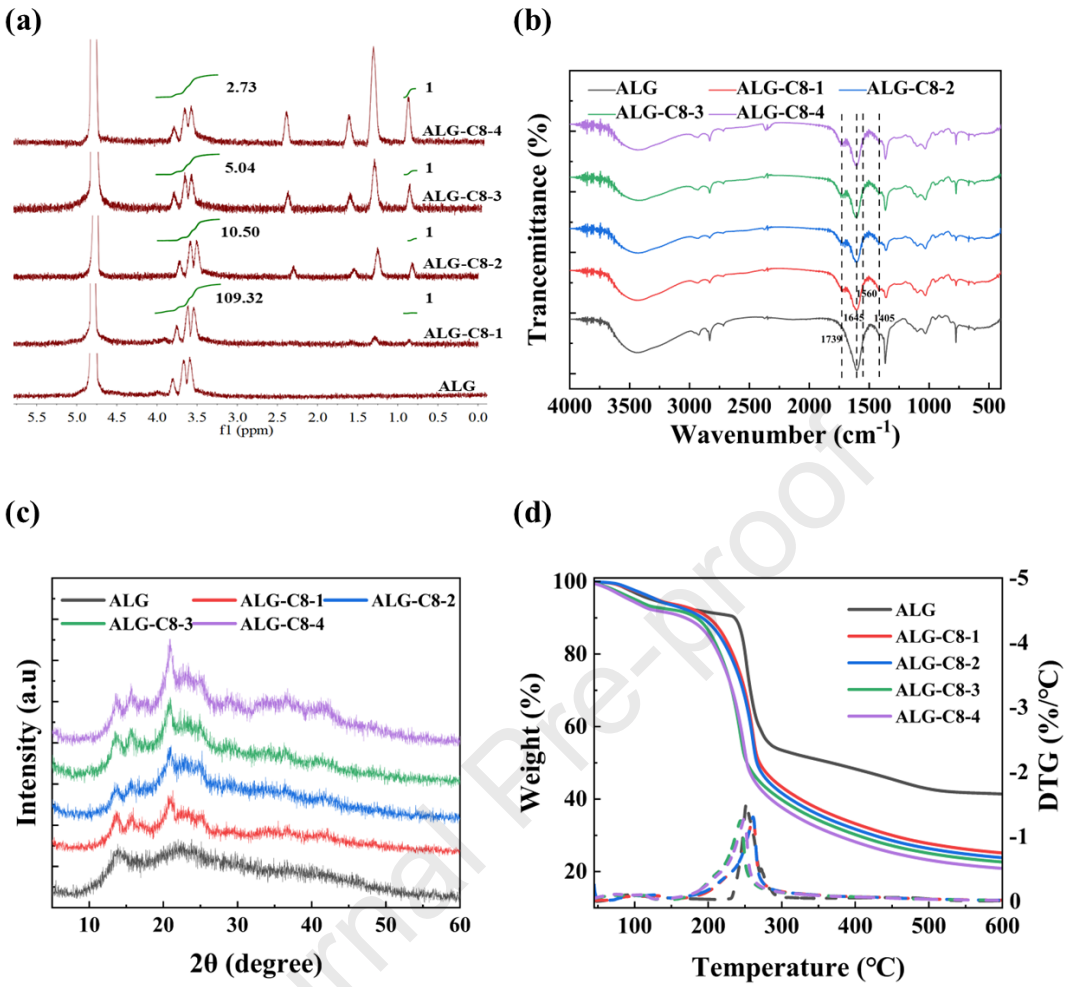

566

567

568 **Fig. 1**

569

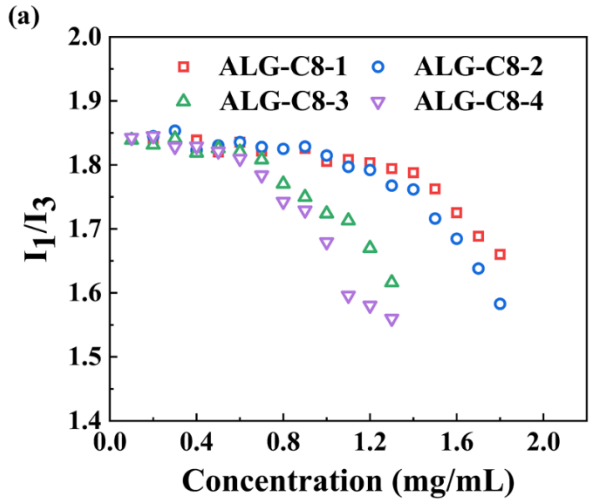

570

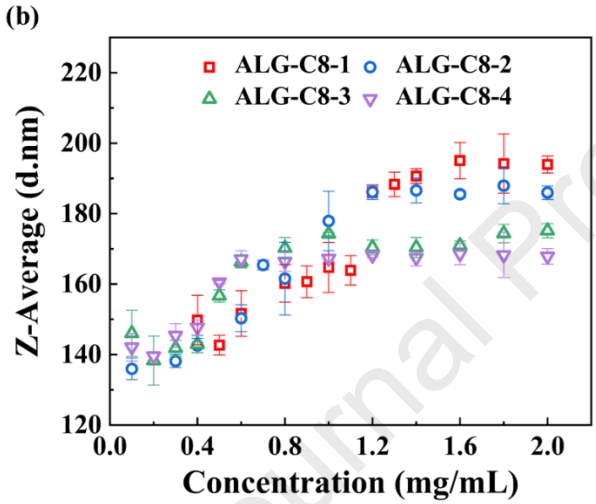

571

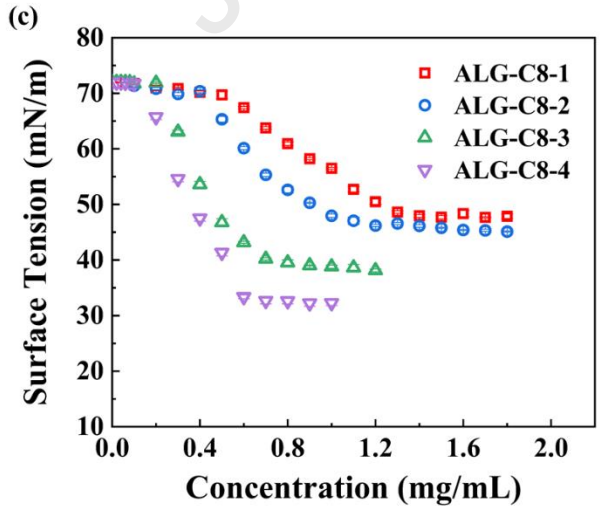

572

573 **Fig. 2**

574

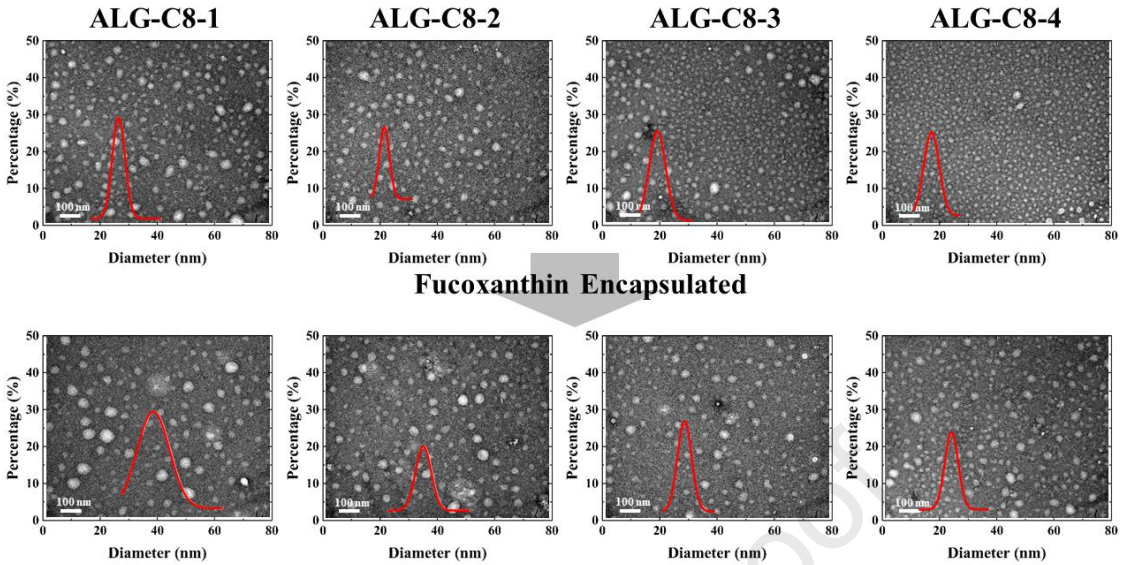

575

576 **Fig. 3**

577

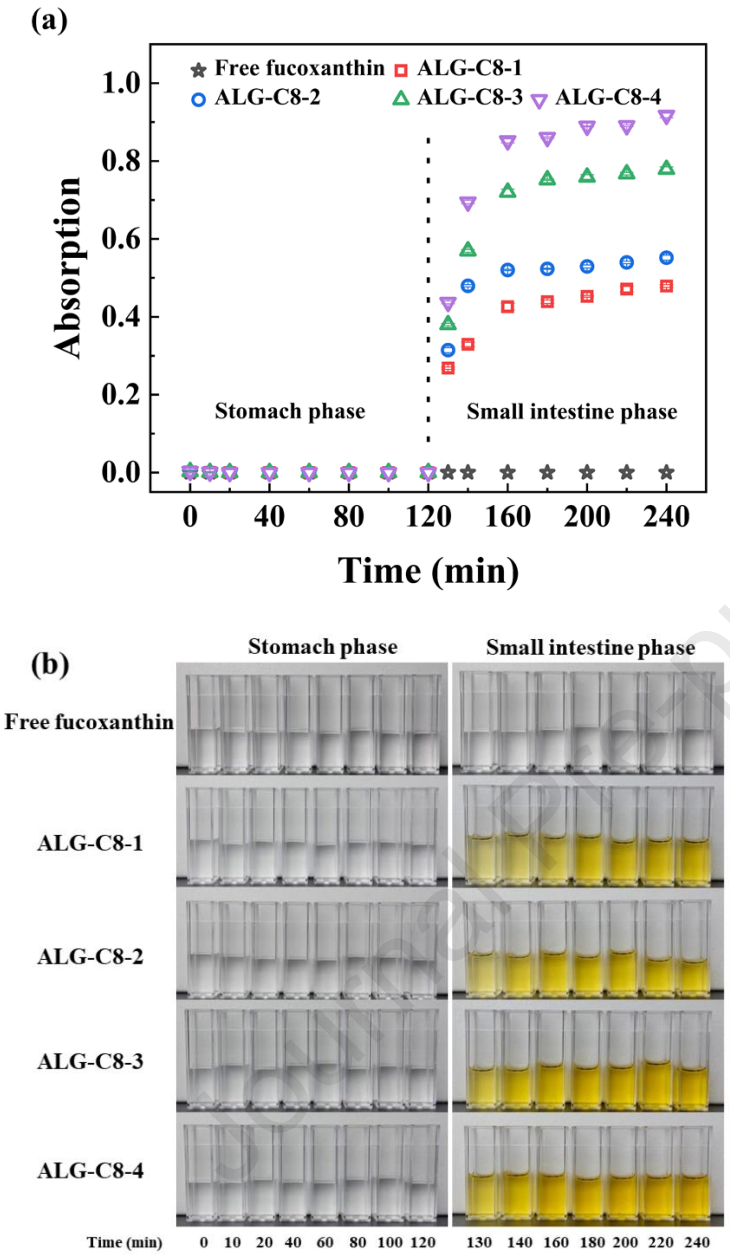

578

579

580

Fig. 4

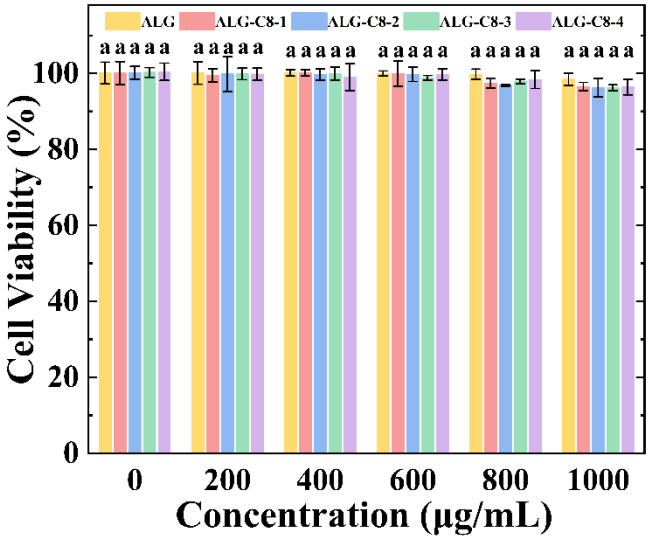

581

582 **Fig. 5**

583

584

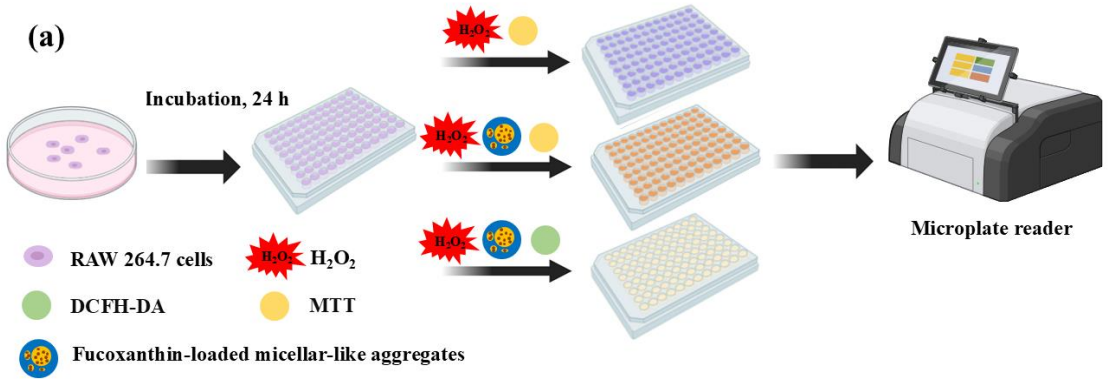

585

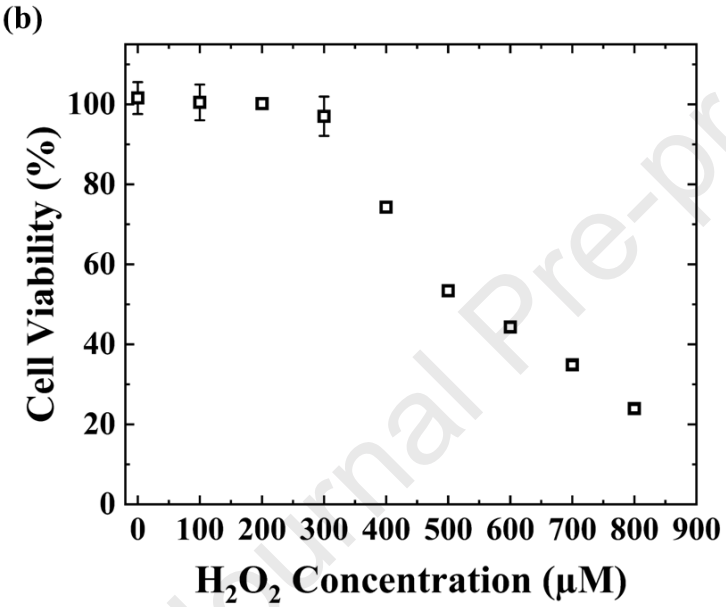

586

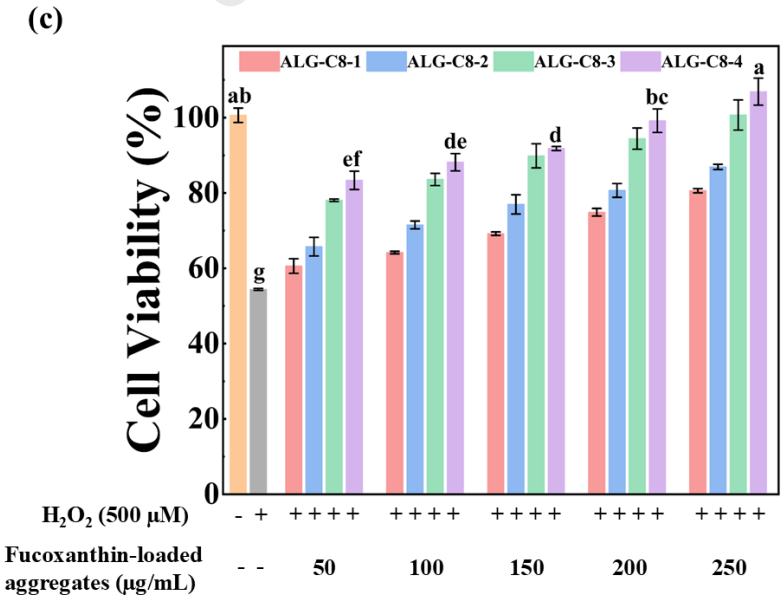

587

588

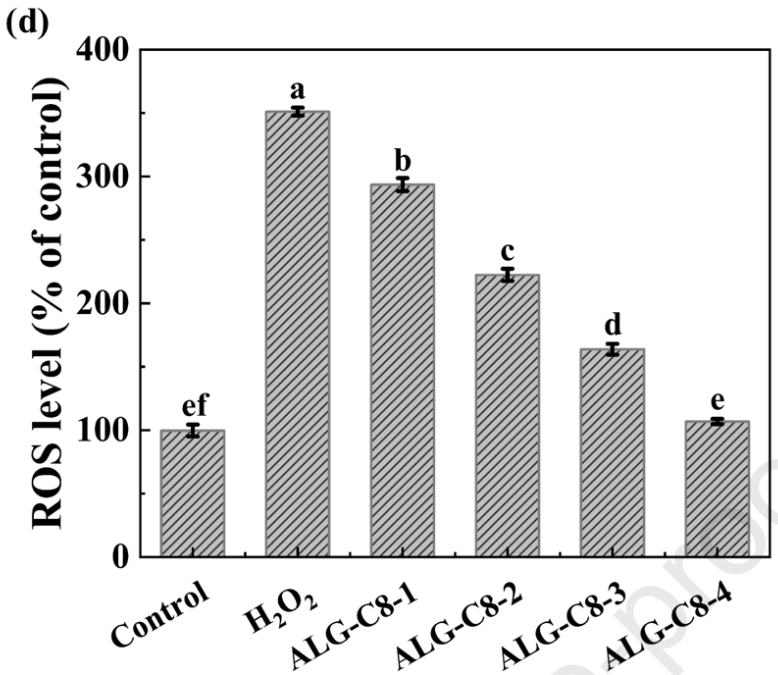

589

590 **Fig. 6**

591

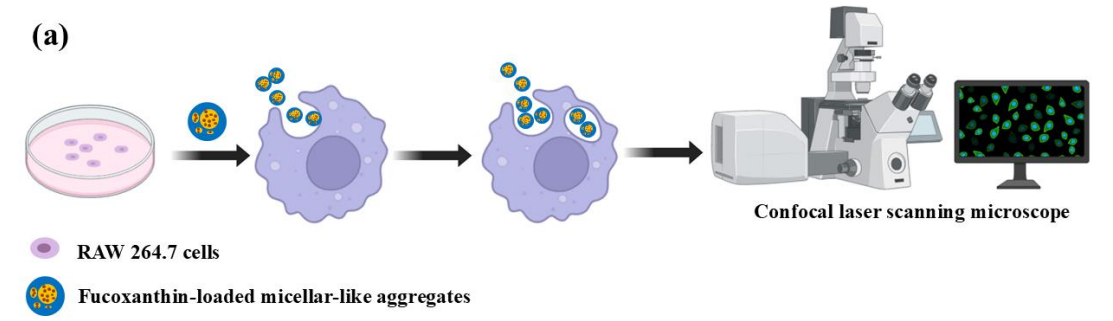

592

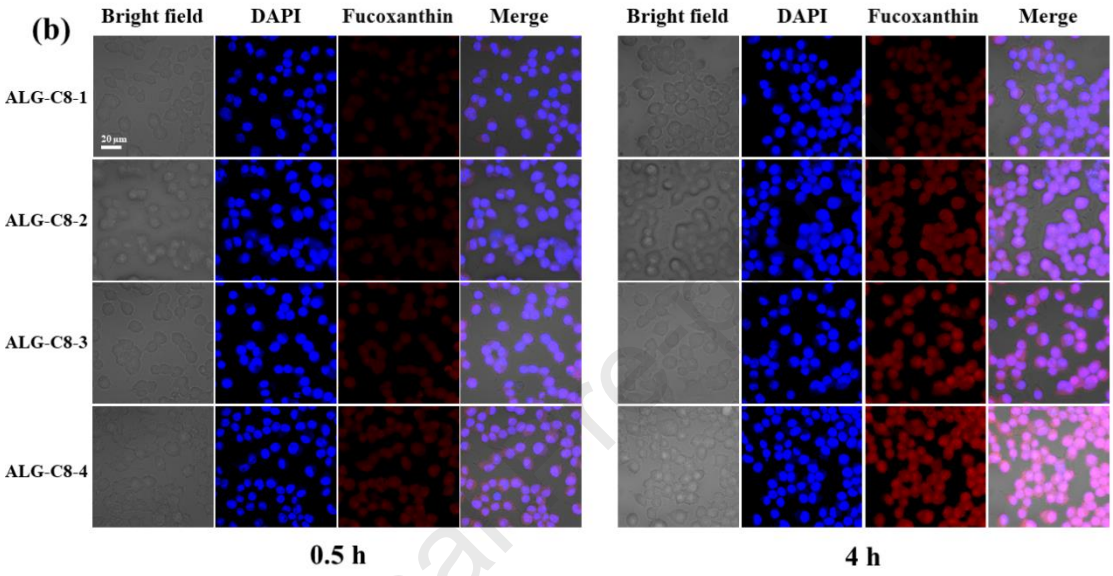

593

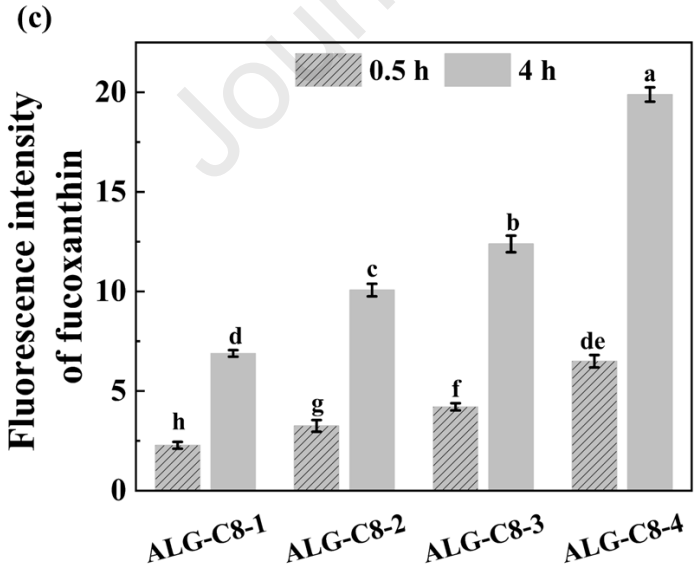

594

595 **Fig. 7**

596

597 **List of Tables**

598 **Table 1.** Properties of ALG-C8 aggregates.

Table 1. Properties of ALG-C8 aggregates

Sample	DS (%)	CAC (mg/mL) Fluorescence measurement	CAC (mg/mL) DLS	CAC (mg/mL) ST	$\Gamma\times10^{-6}$ (mol/m^2)	A (nm^2)	Hydrodynamic Diameters (nm)	Zeta Potential (mV)	EE (%)	LC (%)
ALG-C8-1	1.54 ± 0.04^{d}	1.4	1.43 ± 0.06^{a}	1.37 ± 0.03^{a}	0.08	0.20	193.9 ± 2.40^{a}	-31.3 ± 0.04^{a}	46.11 ± 2.22^{d}	4.61 ± 0.22^{d}
ALG-C8-2	15.50 ± 0.45^{c}	1.1	1.17 ± 0.06^{b}	1.12 ± 0.07^{b}	0.10	0.17	186.0 ± 1.92^{b}	-33.0 ± 0.38^{a}	58.38 ± 0.49^{c}	5.84 ± 0.05^{c}
ALG-C8-3	31.85 ± 1.12^{b}	0.9	0.76± 0.05^{c}	0.73 ± 0.06^{c}	0.11	0.15	175.2 ± 2.01^{c}	-33.2 ± 0.77^{a}	70.32 ± 1.01^{b}	7.03 ± 0.10^{b}
ALG-C8-4	60.20 ± 1.67^{a}	0.5	0.64 ± 0.04^{d}	0.60± 0.05^{d}	0.12	0.14	167.9 ± 2.21^{d}	-33.9 ± 0.89^{a}	88.54 ± 1.14^{a}	8.85 ± 0.11^{a}

Annotation: Values are given as means of triplicate determinations ± standard deviation. Different lowercase represents the significant difference ($p < 0.05$)

599

600 **Reference**

601 Adadi, P., Barakova, N. V., & Krivoshapkina, E. F. (2018). Selected Methods of
602 Extracting Carotenoids, Characterization, and Health Concerns: A Review.
603 *Journal of Agricultural and Food Chemistry, 66*(24), 5925-5947.

604 Akshaya, S., & Nathanael, A. J. (2024). A Review on Hydrophobically Associated
605 Alginates: Approaches and Applications. *ACS Omega, 9*(4), 4246-4262.

606 Barai, M., Mandal, M. K., Karak, A., Bordes, R., Patra, A., Dalai, S., & Panda, A. K.
607 (2019). Interfacial and Aggregation Behavior of Dicarboxylic Amino Acid-
608 Based Surfactants in Combination with a Cationic Surfactant. *Langmuir, 35*(47),
609 15306-15314.

610 Bu, X. T., Ji, N., Dai, L., Dong, X. Y., Chen, M., Xiong, L., & Sun, Q. J. (2021). Self-
611 assembled micelles based on amphiphilic biopolymers for delivery of functional
612 ingredients. *Trends in Food Science & Technology, 114*, 386-398.

613 Fan, Y., Ding, X. T., Wang, L. J., Jiang, E. Y., Van, P. N., & Li, F. L. (2021). Rapid
614 Sorting of Fucoxanthin-Producing Phaeodactylum tricornutum Mutants by
615 Flow Cytometry. *Marine Drugs, 19*(4), 228.

616 Han, L. Y., Ratcliffe, I., & Williams, P. A. (2015). Self-Assembly and Emulsification
617 Properties of Hydrophobically Modified Inulin. *Journal of Agricultural and*
618 *Food Chemistry, 63*(14), 3709-3715.

619 Han, L. Y, Ratcliffe, I., & Williams, P. A. (2017). Synthesis, characterisation and
620 physicochemical properties of hydrophobically modified inulin using long-
621 chain fatty acyl chlorides. *Carbohydrate Polymer, 178*, 141-146.

622 Han, L. Y, Sun, J., Williams, P. A., Yang, J. X., & Zhang, S. B. (2022). Octenyl-
623 succinylated inulins for the delivery of hydrophobic drug. *International Journal*
624 *of Biological Macromolecules, 221*, 1112-1120.

Han, L. Y., Zhai, R. Y., Hu, B., Williams, P. A., Yang, J. X., Zhang, C. Z., Dong, N., & Li, T. T. (2024). Preparation and characterization of hydrophobically-modified sodium alginate derivatives as carriers for fucoxanthin. *Food Hydrocolloids, 157*, 110386.

Han, L. Y., Zhai, R. Y., Hu, B., Yang, J. X., Li, Y. Y., Xu, Z., Meng, Y. Y., & Li, T. T. (2023). Effects of Octenyl-Succinylated Chitosan-Whey Protein Isolated on Emulsion Properties, Astaxanthin Solubility, Stability, and Bioaccessibility. *Foods, 12*(15), 2898.

He, J. R., Zhu, J. J., Yin, S. W., & Yang, X. Q. (2022). Bioaccessibility and intracellular antioxidant activity of phloretin embodied by gliadin/sodium carboxymethyl cellulose nanoparticles. *Food Hydrocolloids, 122*, 107076.

Hua, X., Liu, J. R., Guan, S. Y, Tan, J., Wang, M. M., & Yang, R. J. (2021). Surface activity of ultrahigh methoxylated pectin of different size. *Food Hydrocolloids, 113*, 106495.

Hua, Z., Zhang, X. D., Chen, Y. N., Liu, R. G., Li, Y., Li, J. X., Liu, D. H., & Tan, M. Q. (2023). A bifunctional hepatocyte-mitochondrion targeting nanosystem for effective astaxanthin delivery to the liver. *Food Chemistry, 424*, 136439.

Jian, W. J., Tu, L. Y., Wu, L. L., Xiong, H. J., Pang, J., & Sun, Y. M. (2017). Physicochemical properties and cellular protection against oxidation of degraded Konjac glucomannan prepared by γ-irradiation. *Food Chemistry, 231*, 42-50.

Kuang, H. Y., Ma, L. Y., Guo, Y. J., & Liu, Y. X. (2024). Chitosan surface-modified bovine serum albumin-oleic acid self-assembled complexes: Improving the thermal stability, controlled release and bioaccessibility of fucoxanthin. *Food Hydrocolloids, 151*, 109796.

650 Liang, D., Su, W. T., Zhao, X., Li, J. X., Hua, Z., Miao, S., & Tan, M. Q. (2021).
651 Microfluidic Fabrication of pH-Responsive Nanoparticles for Encapsulation
652 and Colon-Target Release of Fucoxanthin. *Journal of Agricultural and Food*
653 *Chemistry, 70*(1), 124-135.
654 Liu, R. G., Zhang, X. M., Fei, S. Y., & Tan, M. Q. (2024). Orally deliverable lutein
655 nanoparticles as robust ROS scavenger for dry eye disease by targeting Peyer's
656 patches and mitochondria of ocular cell. *Chemical Engineering Journal, 494*,
657 153024.
658 Liu, Z. W., Chen, X. Q., Huang, Z. Q., Shi, J. J., Liu, C. Y., Cao, S. R., Yan, H. Q., &
659 Lin, Q. (2021). Self-assembled oleylamine grafted alginate aggregates for
660 hydrophobic drugs loading and controlled release. *International Journal of*
661 *Polymeric Materials and Polymeric Biomaterials, 72*(3), 212-223.
662 Liu, Z. W., Chen, X. Q., Huang, Z. Q., Wang, H. C., Cao, S. R., Liu, C. Y., Yan, H. Q.,
663 & Lin, Q. (2022). One-Pot Synthesis of Amphiphilic Biopolymers from
664 Oxidized Alginate and Self-Assembly as a Carrier for Sustained Release of
665 Hydrophobic Drugs. *Polymers, 14*(4).
666 Liu, Z. W., Wang, H. C., Bu, Y. N., Wu, T., Chen, X. Q., Yan, H. Q., & Lin, Q. (2024).
667 Fabrication of self-assembled micelles based on amphiphilic oxidized sodium
668 alginate grafted oleoamine derivatives via Schiff base reduction amination
669 reaction for delivery of hydrophobic food active ingredients. *International*
670 *Journal of Biological Macromolecules, 257*, 128653.
671 Lv, Y. Z., Liu, Z. X., Duan, X. Q., Cui, J., Zhang, W. M., Ma, W. R., Liu, Y. Q., Song,
672 X. P., & Fan, Y. P. (2022). Immunoenhancement and antioxidative damage
673 effects of Polygonum Cillinerve polysaccharide on RAW 264.7 cells. *Journal*
674 *of Pharmacy and Pharmacology, 74*(3), 435-445.

675 Mensah, E. O., Kanwugu, O. N., Panda, P. K., & Adadi, P. (2023). Marine fucoidans:
676 Structural, extraction, biological activities and their applications in the food
677 industry. *Food Hydrocolloids, 142*, 108784.
678 Roy, V. C., Haq, M., Ho, T. C., Park, J. S., Chamika, W. A. S., Ali, M. S., Haque, A. R.,
679 Zhang, W., & Chun, B. S. (2024). Important carotenoids derived from marine
680 biomass: Extraction, stabilization, and potentiality in food, cosmetics, and
681 pharmaceutical application. *Food Bioscience, 60*, 104421.
682 Shavronskaya, D. O., Noskova, A. O., Skvortsova, N. N., Adadi, P., & Nazarova, E. A.
683 (2023). Encapsulation of Hydrophobic Bioactive Substances for Food
684 Applications: Carriers, Techniques, and Biosafety, *Journal of Food Processing*
685 *and Preservation, 2023* (1), 5578382.
686 Tian, X. Y., Li, J. X., Wang, K. Y., Fei, S. Y., Zhang, X. M., Wu, C. Y., Tan, M. Q., &
687 Su, W. T. (2024). Microfluidic fabrication of core-shell fucoxanthin nanofibers
688 with improved environmental stability for reducing lipid accumulation in vitro.
689 *Food Chemistry, 442*, 138474.
690 Wang, W., Zhang, F. M., Li, Q., Chen, H., Zhang, W. J., Yu, P., Zhao, T., Mao, G. H.,
691 Feng, W. W., Yang, L. Q., & Wu, X. Y. (2018). Structure characterization of one
692 polysaccharide from Lepidium meyenii Walp., and its antioxidant activity and
693 protective effect against H(2)O(2)-induced injury RAW 264.7 cells.
694 *International Journal of Biological Macromolecules, 118*, 816-833.
695 Wu, Z., Li, H., Zhao, X. W., Ye, F. Y., & Zhao, G. H. (2022). Hydrophobically modified
696 polysaccharides and their self-assembled systems: A review on structures and
697 food applications. *Carbohydrate Polymers, 284*, 119182.
698 Xie, L. M., Huang, Z. B., Qin, L., Yu, Q., Chen, Y., Zhu, H. B., & Xie, J. H. (2022).
699 Effects of sulfation and carboxymethylation on Cyclocarya paliurus

polysaccharides: Physicochemical properties, antitumor activities and protection against cellular oxidative stress. *International Journal of Biological Macromolecules, 204*, 103-115.

Yuan, Y. K., Ma, M. J., & Zhang, S. Z. (2023). Recent advances in delivery systems of fucoxanthin. *Food Chemistry, 404*, 134685.

Zhang, C. C., Zhang, Y., Song, J. F., Wang, H. J, Wu, C., & Li, Y. (2024). Delivery of Lutein by Using Modified Burdock Polysaccharide Aggregates: Preparation, Characterization, and In Vitro Release Properties. *Polymers, 16*(14), 1982.

Highlights

1) A pH- sensitive system for encapsulating fucoxanthin is designed.
2) The ALG-C8 with varying DS formed aggregates in aqueous solution.
3) The sizes of the ALG-C8 aggregates were in the range of 100-200 nm.
4) Both blank and fucoxanthin-loaded ALG-C8 aggregates showed no cytotoxicity.
5) ALG-C8 effectively shielded RAW 264.7 cells from H_2O_2-induced damage.

Declaration of Interest Statement

☒ The authors declare that they have no known competing financial interests or personal relationships that could have appeared to influence the work reported in this paper.

☒ The author is an Editorial Board Member/Editor-in-Chief/Associate Editor/Guest Editor for this journal and was not involved in the editorial review or the decision to publish this article.

☐ The authors declare the following financial interests/personal relationships which may be considered as potential competing interests: